Machine Learning for UAV Classification Employing Mechanical Control Information

AHMED N. SAYED, Graduate Student Member, IEEE
OMAR M. RAMAHI, Fellow, IEEE
GEORGE SHAKER, Senior Member, IEEE
Department of Electrical and Computer Engineering, University of Waterloo, Waterloo, Ontario, Canada

***Abstract*—Range-Doppler images are widely used to classify different types of Unmanned Air Vehicles (UAVs) because each UAV has a unique range-Doppler signature. However, a UAV's range-Doppler signature depends on its movement mechanism. This is why a classifier's accuracy would be degraded if the effect of the mechanical control system of UAVs wasn't taken into consideration, which may lead to a non-unique signature of a UAV while in-flight. In this paper, a full-wave electromagnetic CAD tool is used to investigate the effect of the control systems of two quadcopters, a hexacopter, and a helicopter UAVs on their range-Doppler signatures. A Mechanical Control-Based Machine Learning (MCML) algorithm is introduced to classify the four UAVs. Different Machine Learning (ML) algorithms were applied to the generated datasets that considered the mechanical control information of UAVs. The Convolutional Neural Networks (CNN) algorithms provided robust performance reaching an accuracy of higher than 90%.**

***Index Terms*— UAV Control, Radar, Range-Doppler, Machine Learning, Classification, Drones.**

I. INTRODUCTION

DRONES, or Unmanned Air Vehicles (UAVs), are widely used for illegal activities and terrorist attacks. For example, in 2019, flights were delayed at an airport in the UK due to drone sightings [1], [2]. In 2021, a terrorist organization tried to assassinate the Iraqi Prime Minister using drones [3], while in the same year, another terrorist organization attacked an airport in Turkey [4]. In 2022, a drone attack in the United Arab Emirates killed 3, and injured 6 people [5]. Another drone attack at an airport in Saudi Arabia injured 12 people [6]. Most recently, many flights were delayed in the UK after drone sightings in the vicinity of an airport [7]. It is anticipated that the mobility, cost and easy of operation of drones will be of high appeal to highly organized narcotic cartels and even individual drugs smugglers [8].

Most recently, the war in Ukraine demonstrated how drones are affecting modern warfare. In this war, drones were used for many tasks, from aerial surveillance to missile defense [9], [10]. Drones are capable of carrying explosives, dropping bombs, firing missiles, dropping anti-tanks munitions, aerial photography, and they can be used in Electronic Warfare (EW). This is why detection and classification of drones at a distance is of critical importance in order to have enough time to take necessary counter-measures.

To detect drones, radar systems are typically preferred in comparison to other systems. This is because radar systems can work day and night and in all weather conditions. They can also detect and track multiple drones, track autonomous flights, and have the potential to classify different targets when combined with Machine Learning (ML) algorithms [11]–[16].

Range Doppler (RD) images are widely used to classify radar targets [17]–[19]. Each drone has its own set of unique RD signatures that depend on the drone's movement mechanism. Typically, drones have eight main unique movements: the drone is able to throttle up, throttle down, pitch forward, pitch backward, roll left, roll right, yaw left, and yaw right. These different motions are performed by changing individually the speed of each rotor.

The RD signature of each movement of a drone differs from the RD signature for the other movements. If a classifier was trained on specific movements only, the error in drones' classification would be higher if the classifier was tested on different movements from those on which it was trained. This is the case in all previous works, where ML algorithms were trained and tested using the same datasets. These datasets simply did not consider the effect of the mechanical control information of the drones on their RD images.

Full-wave electromagnetic (EM) simulation software can be used to generate radar drones' datasets [20]. In this work, Ansys High-Frequency Structure Simulator (HFSS) [21], [22] is used to investigate the effect of the mechanical control systems on the RD signatures of drones. For validation, four different drones are considered in this work: the MD-1000 quadcopter drone [23], the DJIFPV quadcopter drone [24], the DJI S900 hexacopter drone [25], and the Black Eagle 50 helicopter drone [26]. To create RD images for the designed dataset, the Shooting and Bouncing Rays SBR+ technique (in HFSS) is used. It is an asymptotic high-frequency electromagnetic (EM) simulator for modeling EM interaction [27]. In this work, a 77 GHz FMCW radar, modeled in HFSS, was used to generate the datasets, as short-range radars are widely

Manuscript received XXXXX 00, 0000; revised XXXXX 00, 0000; accepted XXXXX 00, 0000.
(Corresponding author: Ahmed N. Sayed)

Ahmed N. Sayed, Omar M. Ramahi, and George Shaker are with the Department of Electrical and Computer Engineering, University of Waterloo, Waterloo, Ontario, Canada. (e-mail: ansayed@uwaterloo.ca, oramahi@uwaterloo.ca, gshaker@uwaterloo.ca)

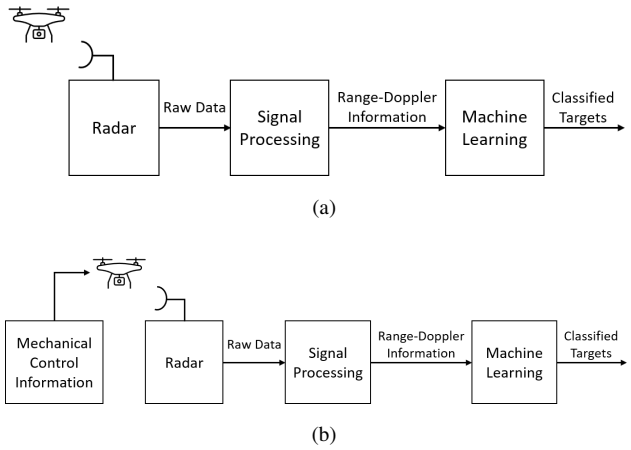

Fig. 1: (a) Traditional Method. (b) Proposed MCML Method.

used because of their high accuracy in detecting RD signatures.

The following is a summary of the contributions in this article:

1) Generating radar datasets that contain drones without constraints using full wave EM CAD tools.
2) Applying ML algorithms to the datasets generated by full-wave EM CAD tools.
3) An investigation of the effect of the mechanical control information of drones on the RD signatures of drones and the accuracy of ML classifiers is conducted. A Mechanical Control-Based Machine Learning (MCML) algorithm is proposed to avoid degradation in ML accuracy when ignoring the mechanical control information of drones. Fig. 1 (a) shows the traditional method, while Fig. 1 (b) shows the proposed MCML method.
4) An investigation and comparison between different classifiers on radar drones' datasets considering the mechanical control information of drones is presented.

The paper is organized as follows: in section II the mathematical models of the control systems for the quadcopter and the hexacopter drones are presented. In section III, the radar parameters, the drones' specifications, the simulation setups for different movements of the drones, and the simulation results that contain the RD signatures for different cases of the drones movements are introduced. The classification results and a validation of the MCML algorithm are shown in section IV. A conclusion follows in section V.

II. MATHEMATICAL MODELS

This section describes the mathematical model of the equations of motions for the quadcopter and the hexacopter drones in different motions. The equations of motions for the helicopter drone can be found in [28].

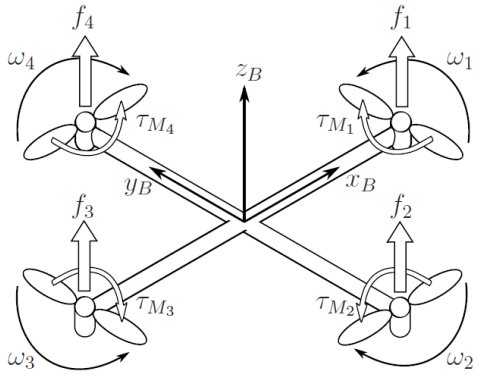

Fig. 2: The quadcopter frame body [29].

A. Quadcopter Equations of Motions

The quadcopter is controlled by changing the angular velocities of the rotors. Basically, a quadcopter is a 4-rotor helicopter. Its thrust to hover or throttle is provided by the four rotors equally, while other movements can be controlled by changing the motors' speeds. The four rotors of a quadcopter are arranged clockwise (CW) and counter-clockwise (CCW) that work together to provide stability, and all required movements. Quadcopters hover in the air, throttle up and down, roll left and right, and yaw left and right.

The body frame of a quadcopter is shown in Fig. 2 [29]. The forces and moments on a quadcopter are given as [29], [30]:

$$F_i = K_f \times \omega_i^2 \tag{1}$$

$$M_i = K_m \times \omega_i^2 \tag{2}$$

where F_i is the lifting force for each propeller, M_i is the moment at each propeller, $i = 1, 2, 3, 4$, K_f and K_m are the aerodynamics force and moment constants, and ω_i is the angular speed for each propeller.

The resultant thrust by opposite propellers generates moments in x and y axes, M_x and M_y:

$$M_y = (F_2 - F_4) \times L \tag{3}$$

$$M_x = (F_1 - F_3) \times L \tag{4}$$

where L is the length between the two propellers. mg is the gravity force that acts in the opposite direction of the thrust.

According to Newton's second law of motion [30], the linear and rotational motions of a quadcopter can be expressed as:

$$Force = mass \times linear\ acceleration \tag{5}$$

$$Torque = inertia \times angular\ acceleration \tag{6}$$

Since inertia is the object's resistance to change, while in motion, as the momentum increases, the inertia increases. The linear motion of a quadcopter is represented in (5), while (6) represents the rotational motion.

When a quadcopter hovers, all the forces applied on it must be in balance, which means the total lifting

force equals its weight. Additionally, the conservation of momentum gives:

$$mg = F_1 + F_2 + F_3 + F_4 \tag{7}$$

The equation of motion for a hovering quadcopter is:

$$m\frac{\partial^2 r}{\partial t^2} = F_1 + F_2 + F_3 + F_4 - mg = 0 \tag{8}$$

where m is the mass of the quadcopter, and r is the position.

For a quadcopter to throttle up and throttle down, its equations of motion are given as:

$$m\frac{\partial^2 r}{\partial t^2} = \begin{cases} F_1 + F_2 + F_3 + F_4 - mg > 0 & F > mg \\ F_1 + F_2 + F_3 + F_4 - mg < 0 & F < mg \end{cases} \tag{9}$$

where the total lifting force $F = F_1 + F_2 + F_3 + F_4$, in addition, $all\ moments = 0$. On the other hand, in yaw motions, $all\ moments \neq 0$, while $F = mg$, then:

$$m\frac{\partial^2 r}{\partial t^2} = F_1 + F_2 + F_3 + F_4 - mg = 0 \tag{10}$$

$$I_{ZZ}\frac{\partial^2 \psi}{\partial t^2} = M_1 + M_2 + M_3 + M_4 \tag{11}$$

where the yaw, ψ, pitch, θ, and roll,vϕ, are called the Euler angles [30]. These angles describe the angular orientation of a fixed body with respect to a reference frame. Due to the quadcopter symmetrical frame, the inertia matrix I is given as:

$$I = \begin{bmatrix} I_{XX} & 0 & 0 \\ 0 & I_{YY} & 0 \\ 0 & 0 & I_{ZZ} \end{bmatrix} \tag{12}$$

Finally, in pitch and roll motions, $all\ moments \neq 0$, and $mg < F$. The pitch and roll angles must be nonzero; this causes nonzero components of thrust in the horizontal direction, which causes a resultant moment in the horizontal plane. The equations of motion become:

$$m\frac{\partial^2 r}{\partial t^2} = F_1 + F_2 + F_3 + F_4 - mg > 0 \tag{13}$$

$$I_{XX}\frac{\partial^2 \phi}{\partial t^2} = (F_1 - F_3) \times L \tag{14}$$

$$I_{YY}\frac{\partial^2 \theta}{\partial t^2} = (F_2 - F_4) \times L \tag{15}$$

B. Hexacopter Equations of Motions

Similar to the quadcopter drone, the hexacopter drone is controlled by changing the angular velocities of the rotors; however, it provides more flight time, and has the ability to carry more load. It can be considered a 6-rotor helicopter. Its thrust is provided by the six rotors equally, while other movements can be controlled by changing the motors' speeds. A The rotors of a hexacopter are arranged CW and CCW that work together to provide stability, and all required movements for a hexacopter [31].

The body frame of a hexacopter is shown in Fig. 3 [32]. According to [30]–[32], the forces and moments on a hexacopter follow equations (1) and (2).

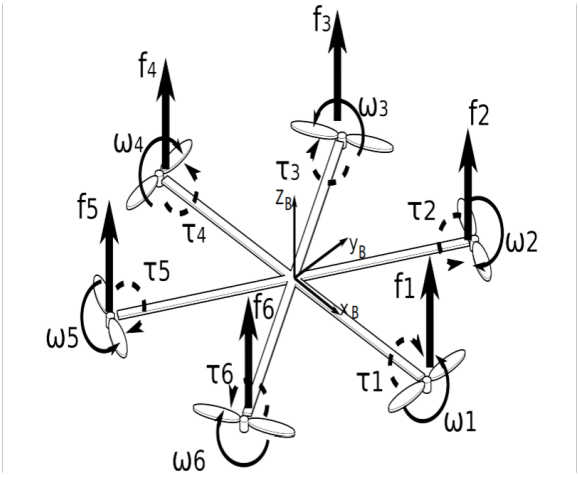

Fig. 3: The hexacopter frame body [32].

The resultant moment for a hexacopter is given by:

$$M = r_1F_1 + r_2F_2 + r_3F_3 + r_4F_4 + r_5F_5 + r_6F_6 \tag{16}$$

where F_i is the lifting force for each propeller, and r_i is the radius from the center of the hexacopter to each propeller, $i = 1, 2, 3, 4, 5, 6$.

The equation of motion for a hovering hexacopter is given as:

$$m\frac{\partial^2 r}{\partial t^2} = F_1 + F_2 + F_3 + F_4 + F_5 + F_6 - mg = 0 \tag{17}$$

For a hexacopter to throttle up and throttle down, its equations of motion are given as:

$$m\frac{\partial^2 r}{\partial t^2} = \begin{cases} F - mg > 0 & F > mg \\ F - mg < 0 & F < mg \end{cases} \tag{18}$$

where the total lifting force $F = F_1 + F_2 + F_3 + F_4 + F_5 + F_6$, $all\ moments = 0$. In yaw motions, $all\ moments \neq 0$, while $F = mg$, and the total torque in the z-axis can be obtained by increasing/decreasing the CW rotors speeds while decreasing/increasing the CCW rotors speed. The equation of motion for the yaw motion is given as:

$$m\frac{\partial^2 r}{\partial t^2} = F_1 + F_2 + F_3 + F_4 + F_5 + F_6 - mg = 0 \tag{19}$$

Finally, in pitch and roll motions, $all\ moments \neq 0$, and $mg < F$. The pitch and roll angles must be nonzero; this causes nonzero components of thrust in the horizontal direction, which causes the resultant moment to be in the horizontal plane. The pitch motion is achieved by increasing/decreasing the rear rotors' speeds while decreasing/increasing the front rotors' speeds. Roll motion is achieved by increasing/decreasing the side rotors' speeds while decreasing/increasing the other side rotors' speeds. The equation of motion becomes:

$$m\frac{\partial^2 r}{\partial t^2} = F_1 + F_2 + F_3 + F_4 + F_5 + F_6 - mg > 0 \tag{20}$$

The torques applied on the hexacopter body around the roll, pitch, and yaw angles given by

$$\tau_\phi = \frac{3}{4}K_f r({\omega_2}^2 + {\omega_3}^2 - {\omega_5}^2 - {\omega_6}^2) \tag{21}$$

TABLE I: Used Radar Parameters.

Quantity	Symbol	Value
Center Frequency	f_0	77 GHz
Bandwidth	BW	2 GHz
Range Resolution	ΔR	0.075 m
Velocity Resolution	ΔV	0.52 m/s
Maximum Range	R_{max}	60 m

TABLE II: Drones Dimensions.

Drone	Type	Dimensions
MD4-1000	Quadcopter A	1.136 m x 1.730 m x 0.495 m
DJIFPV	Quadcopter B	0.178 m x 0.232 m x 0.127 m
DJI S900	Hexacopter	Diagonal 0.9 m, Arm 0.358 m
Black Eagle	Helicopter	2.65 m x 0.56 m, rotor 3.75 m

$$\tau_\theta = K_f r(-{\omega_1}^2 - \frac{{\omega_2}^2}{4} + \frac{{\omega_3}^2}{4} + {\omega_4}^2 + \frac{{\omega_5}^2}{4} - \frac{{\omega_6}^2}{4}) \quad (22)$$

$$\tau_\psi = b(-{\omega_1}^2 + {\omega_2}^2 - {\omega_3}^2 + {\omega_4}^2 - {\omega_5}^2 + {\omega_6}^2) \quad (23)$$

where b is a constant.

As shown in (1) and (2), by mechanically controlling the speeds of the drones' rotors, the behavior or movement for the quadcopter and the hexacopter drones changes, which also affects the RD signatures for these drones.

III. SIMULATION SETUPS

The radar parameters that were used in this work are shown in Table I. Four different drones were modeled using HFSS, the MD4-1000 quadcopter drone, the DJIFPV quadcopter drone, the Black Eagle 50 helicopter drone, and the DJI S900 hexacopter drone. The dimensions for these drones are shown in Table II. Fig. 4 (a). Fig. 4 (b) show the DJI S900 hexacopter drone [25] and its model in HFSS. The MD4-1000 quadcopter drone, the DJIFPV quadcopter drone, and the Black Eagle 50 helicopter drone shown in Fig. 5 are modeled using a similar approach. HFSS test setups for the different movements for the four drones are shown in Fig. 7 (a-d). The radar, drones, drones' moving directions, drones' moving speeds, and rotors RPM are all modeled using HFSS. To throttle the drone up, the rotors must have the same speed, which is modeled to be high enough to generate a resultant thrust that exceeds the weight of the drone, while to throttle down, the rotors' speeds are modeled with a lower speed as shown in Fig. 7 (a). To pitch the drone forward, its back rotors must have higher speeds than the front rotors, and vice versa to pitch the drone backward as shown in Fig. 7 (b). To roll the drone left, the right rotors must have higher speeds then the left rotors, and vice versa to roll the drone right as shown in Fig. 7 (c). Each rotor rotates in a different direction to the one beside it to keep the drone stable. To yaw the drone left, the CCW rotors must have higher speeds than the CW rotors, and vice versa to yaw the drone right as shown in Fig. 7 (d). For instance, Fig. 6 summarizes the different motions with the rotors speeds for a quadcopter [33].

As shown in Fig. 7 (a), the drones are 30 m away from the radar; they throttle up for a distance of 25 m,

(a)

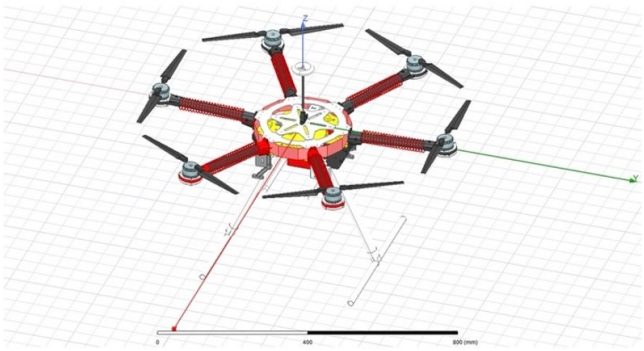

(b)

Fig. 4: (a) The DJI S900 hexacopter drone [25]. (b) Its HFSS model.

(a)

(b)

(c)

Fig. 5: (a) The MD4-1000 quadcopter drone [23]. (b) The DJIFPV quadcopter drone [24]. (c) The Black Eagle 50 helicopter drone [26].

This article has been accepted for publication in IEEE Transactions on Aerospace and Electronic Systems. This is the author's version which has not been fully edited and content may change prior to final publication. Citation information: DOI 10.1109/TAES.2023.3272303

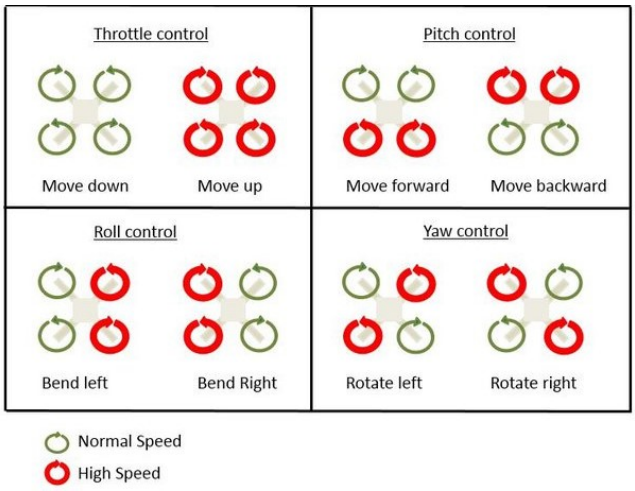

Fig. 6: Quadcopter control [33].

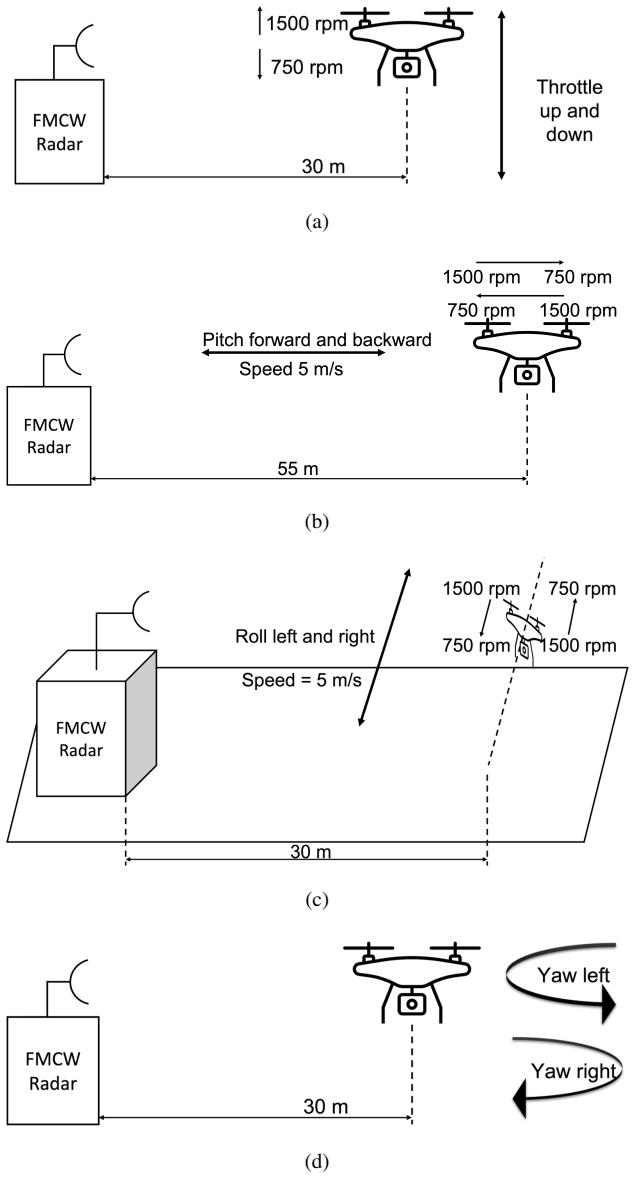

Fig. 7: HFSS test setups for the drones different movements. (a) Throttle up and down. (b) Pitch forward and backward. (c) Roll left and right. (d) Yaw left and right.

TABLE III: Generated Datasets.

Dataset	Control Motions	RD images
Dataset 1	Throttle and Pitch	1200 (300/drone)
Dataset 2	Roll and Yaw	1600 (400/drone)
Dataset 3	Throttle, Pitch, Roll, and Yaw	2800 (700/drone)
Dataset 4	Random *all* motions	3000 (750/drone)

with rotors' speeds equal to 1500 RPM. They throttle down with rotors' speeds equal to 750 RPM. As shown in Fig. 7 (b), the drones pitch forward towards the radar with a fixed speed of 5 m/s, from 55 m to 5 m away from the radar, with back rotors speeds equal to 1500 RPM and forward rotors speeds equal to 750 RPM. Also, they pitch backward with the same speed of 5 m/s from 5 m to 55 m, with back rotors' speeds equal to 750 RPM and forward rotors' speeds equal to 1500 RPM. The drones roll left at 30 m away from the radar for a distance of 50 m. The right rotors' speeds equal to 1500 RPM and left rotors' speeds equal to 750 RPM. They roll right with the right rotors' speeds equal to 750 RPM and the left rotors' speeds equal to 1500 RPM, as shown in Fig. 7 (c). Finally, as shown in Fig. 7 (d), the drones yaw left at 30 m away from the radar with the CCW rotors speeds equal to 1500 RPM and the CW rotors' speeds equal to 750 RPM. They yaw right with the CCW rotors' speeds equal to 750 RPM and the CW rotors' speeds equal to 1500 RPM.

Fig. 8, Fig. 9, and Fig. 10 show the effect of the mechanical control information on the RD images of the MD4-1000 quadcopter drone and the DJI S900 hexacopter drone *only* as examples of the effect of the mechanical control information of drones on their RD images. The required radar datasets for the four drones were generated using the RD images which were generated using Ansys HFSS. The simulation setups used for all the different cases in which the drones move are shown in Fig. 7 (a-d). A 77 GHz FMCW radar was modeled in HFSS; its chosen parameters are shown in Table I. The RD images for each drone were extracted from HFSS to create the required datasets. For each drone, 700 frames were extracted, with a total of 2800 frames in the generated dataset. The extracted frames were normalized, and a threshold was applied to them.

In this work, four different datasets were utilized, all of which were generated using Ansys HFSS and contain the range-Doppler images pertaining to four types of drones investigated in this study. The first dataset comprises 1200 range-Doppler images, with 300 images corresponding to each drone, and encompasses pitch forward, pitch backward, throttle up, and throttle down movements, as illustrated in Fig. 7 (a, b). The second dataset comprises 1600 range-Doppler images, with 400 images for each drone, and encompasses roll left, roll right, yaw left, and yaw right movements, as depicted in Fig. 7 (c, d). The third dataset encompasses all types of movements with varying speeds, and includes 2800 range-Doppler images, with 700 images for each drone. The fourth dataset was employed to validate the proposed approach. It includes range-Doppler images of the four

This article has been accepted for publication in IEEE Transactions on Aerospace and Electronic Systems. This is the author's version which has not been fully edited and content may change prior to final publication. Citation information: DOI 10.1109/TAES.2023.3272303

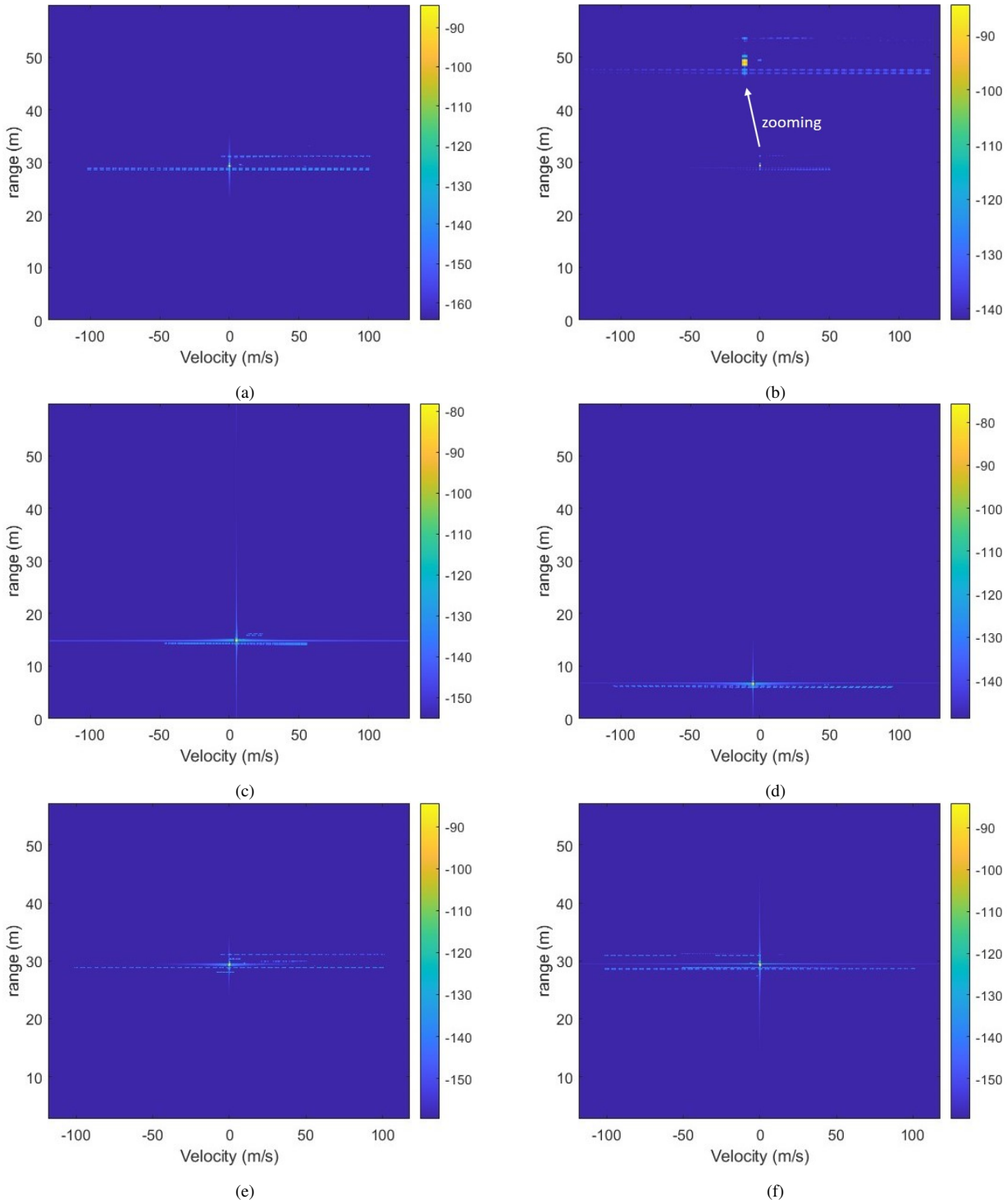

Fig. 8: (a) RD image for throttle up quadcopter. (b) RD image for throttle down quadcopter. (c) RD image for pitch forward quadcopter. (d) RD image for pitch backward quadcopter. (e) RD image for roll left quadcopter. (f) RD image for roll right quadcopter.

drones with randomized motions with varying speeds, as illustrated in Fig. 16.

The number of range-Doppler images in each dataset depends on the number of modeled motions and the number of range-Doppler images for each motion. The datasets are divided into 80% training set and 20% test set. Table III presents a summary of the types of motions in the four datasets utilized in this study, along with the number of frames contained in each dataset.

IV. CLASSIFICATION RESULTS

Eight different ML algorithms were applied to the dataset generated according to Fig. 7 (a-d) to investigate and compare their performance on classifying the four drones. The MD4-1000 quadcopter drone, the DJIFPV quadcopter drone, the DJI S900 hexacopter drone, and the Black Eagle 50 helicopter drone are denoted as Quad A, Quad B, Hexa, and Heli respectively. The eight classifiers

This article has been accepted for publication in IEEE Transactions on Aerospace and Electronic Systems. This is the author's version which has not been fully edited and content may change prior to final publication. Citation information: DOI 10.1109/TAES.2023.3272303

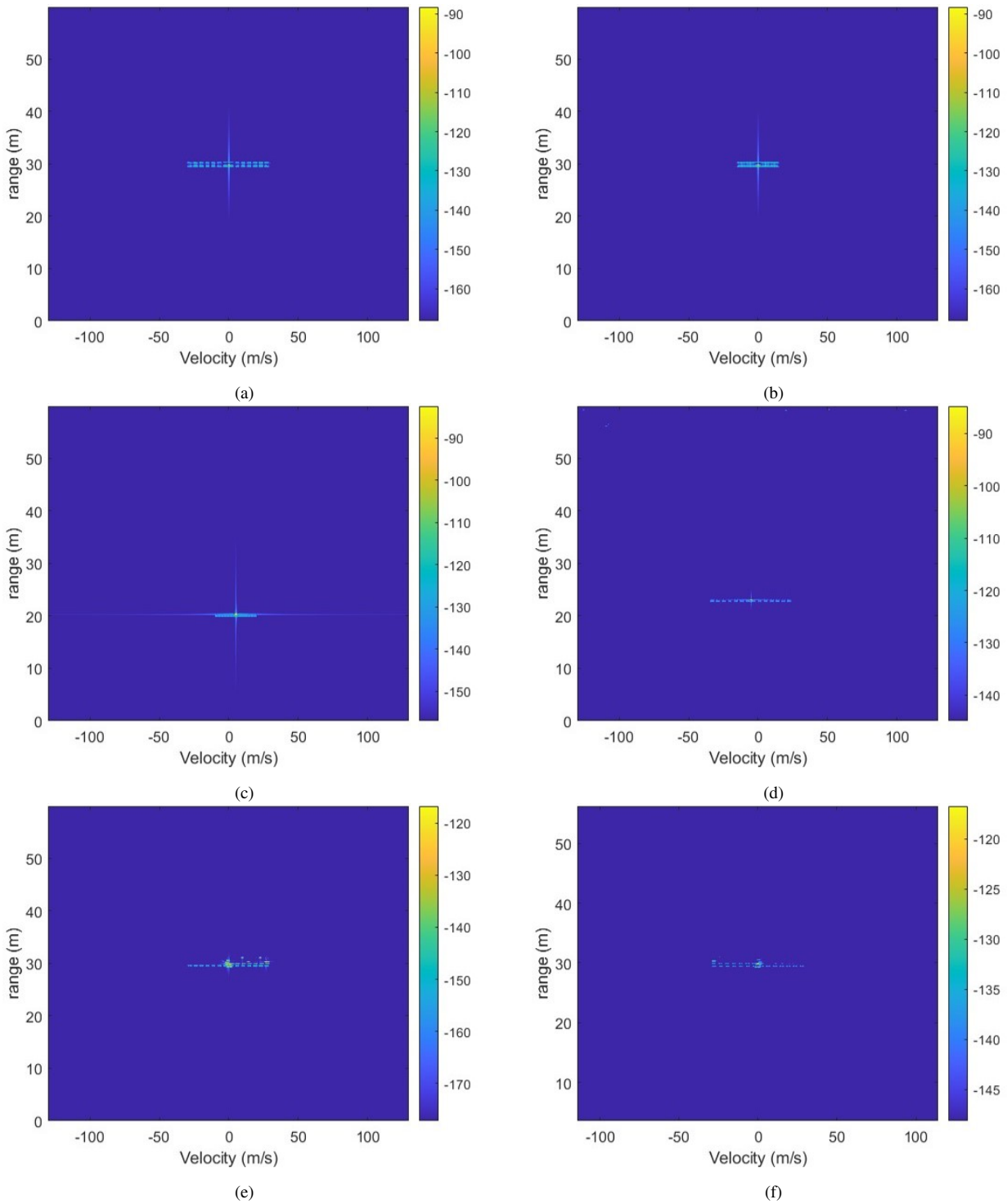

Fig. 9: (a) RD image for throttle up hexacopter. (b) RD image for throttle down hexacopter. (c) RD image for pitch forward hexacopter. (d) RD image for pitch backward hexacopter. (e) RD image for roll left hexacopter. (f) RD image for roll right hexacopter.

are 3 different CNN algorithms, Support Vector Machine (SVM), K-nearest neighbors (KNN), Naive Bayes (NB), Random Forest (RF), and Decision Tree (DT) classifiers.

The classification accuracy for the eight ML algorithms decreased when the mechanical control information of drones were not taken into consideration, while the eight ML algorithms performed well when they considered *all* the mechanical control information of drones as shown in Fig. 12. CNNs are powerful algorithms that are frequently used for radar targets classification [34], [35]. Fig. 12 shows the accuracy of different machine learning algorithms. The three most accurate algorithms are the DopplerNet algorithm [34], denoted as CNN1, the VGG16 algorithm [36], denoted as CNN2, and the light CNN algorithm [37], denoted as CNN3. For a more detailed investigation, the classification reports for

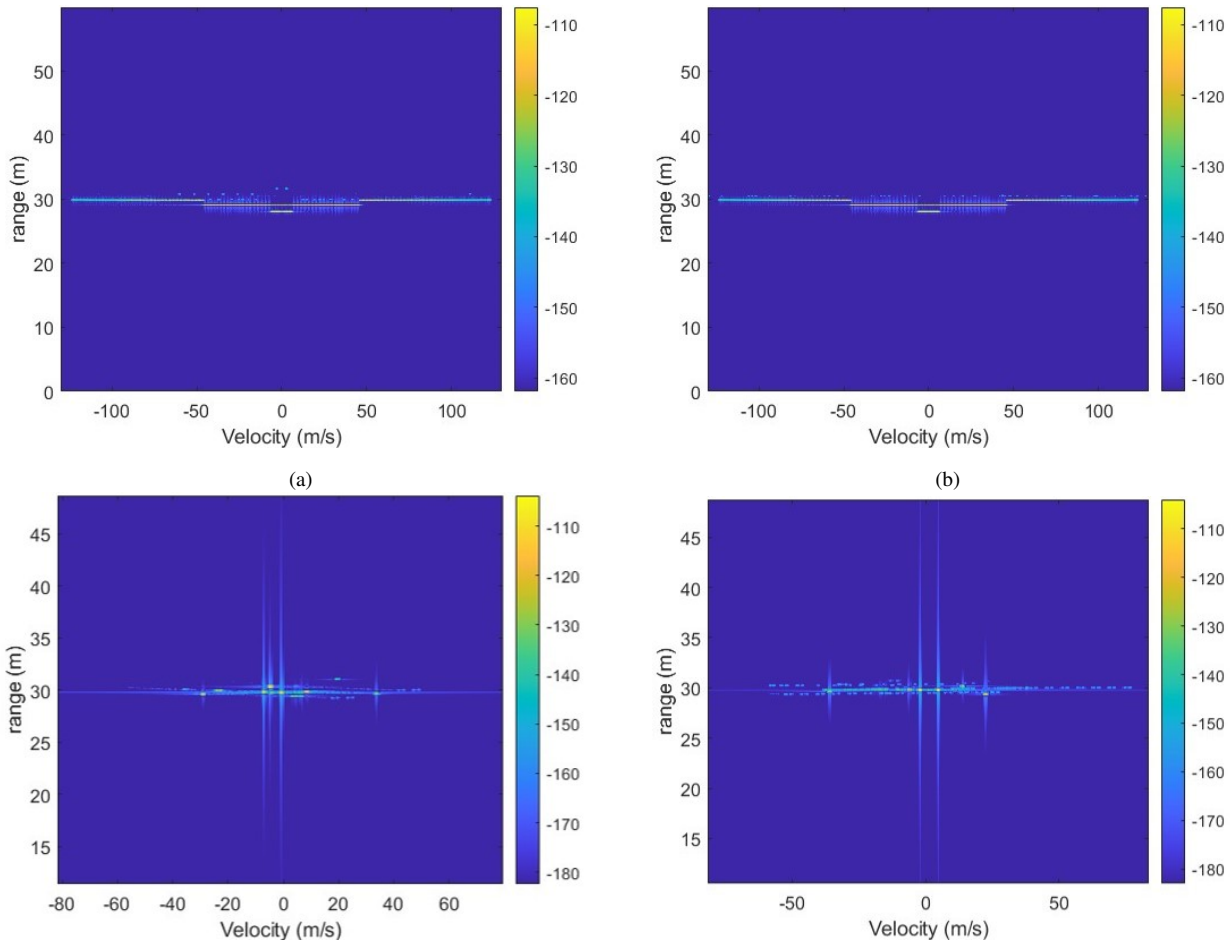

Fig. 10: (a) RD image for yaw left quadcopter. (b) RD image for yaw right quadcopter.(c) RD image for yaw left hexacopter. (d) RD image for yaw right hexacopter.

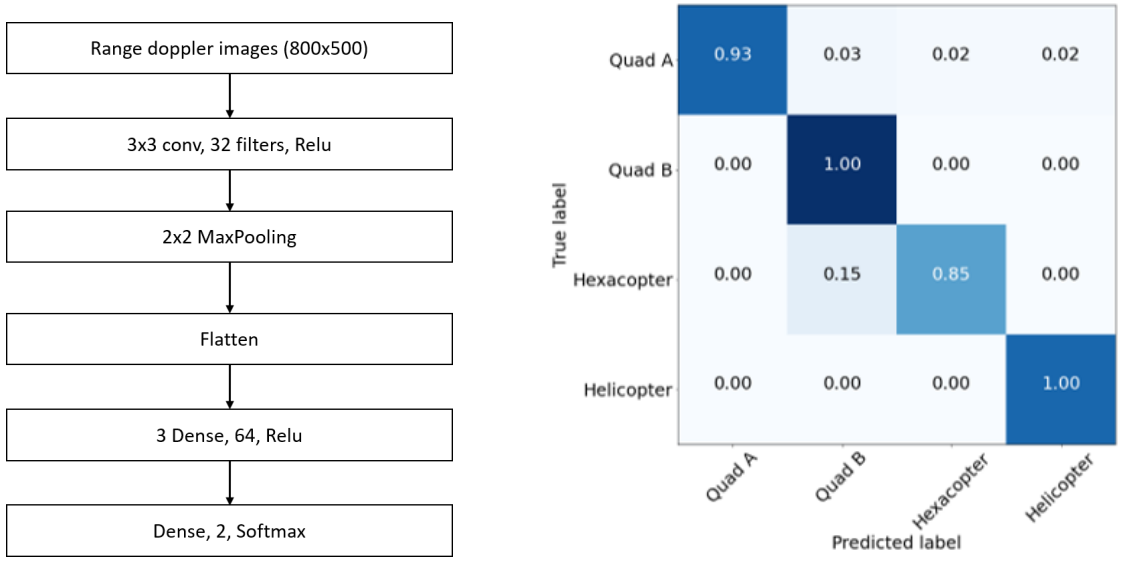

Fig. 11: (a) A flowchart of the DopplerNet CNN algorithm. (b) Its confusion matrix when it was applied on the same dataset.

the three CNN classifiers are shown in Fig. 14 (a) and Fig. 14 (b) when the mechanical control information of drones was not taken into consideration and when it was taken into consideration, respectively.

This article has been accepted for publication in IEEE Transactions on Aerospace and Electronic Systems. This is the author's version which has not been fully edited and content may change prior to final publication. Citation information: DOI 10.1109/TAES.2023.3272303

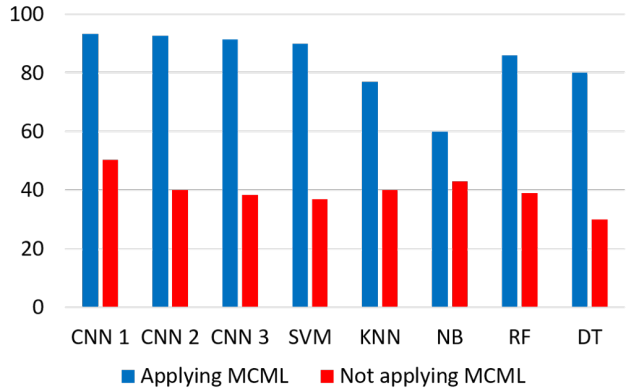

Fig. 12: Different classifiers accuracy when considering/Not considering the mechanical control information of drones.

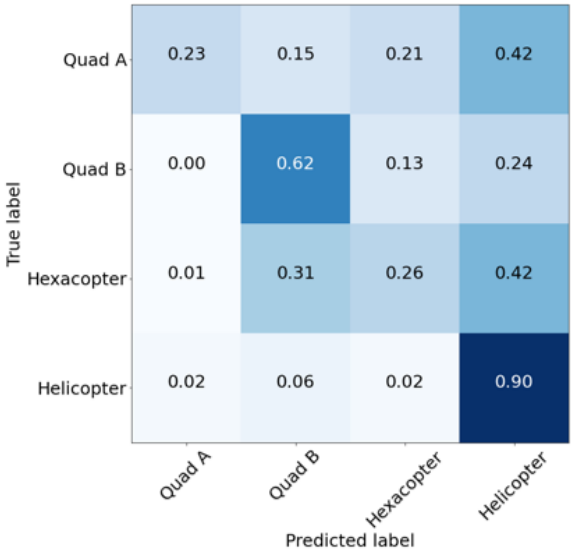

(a)

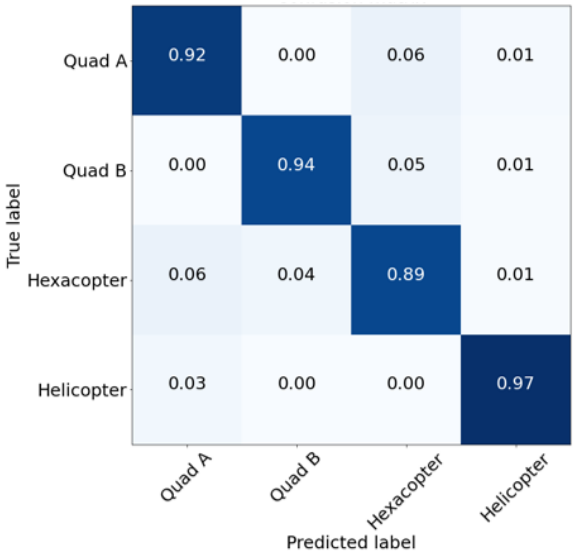

(b)

Fig. 13: Confusion matrix for the DopplerNet CNN algorithm when (a) Not considering the mechanical control information of drones. (b) Considering the mechanical control information of drones.

The classification reports for the CNN classifiers focus only on the quadcopters and the hexacopter drones as the helicopter drone is easily differentiated because it has larger Radar Cross Section (RCS) area than the other drones. The three most accurate CNN algorithms were modified to match the RD images dimensions. The DopplerNet algorithm was found to have slightly higher accuracy than the other two CNN algorithms. Therefore, it was used to classify the four drones. A Maxpooling layer is added to this algorithm to decrease its complexity to avoid over-fitting. The flow chart for this algorithm, which consists of eight layers, is shown in Fig. 11 (a).

According to the chosen range and velocity resolutions shown in Table I, the input layer's dimension was 800 $\times$ 500. A convolutional layer with 32 filters, a 3 $\times$ 3 kernel, and Relu activation function yields an output having a size of 798 $\times$ 498 $\times$ 32. A Maxpooling, 2 $\times$ 2, layer follows the convolutional layer, its output size is 399 $\times$ 249 $\times$ 32. A flatten layer is used to reshape the previous feature map into a vector, its output size is 3,179,232. Four dense layers are used, three of them use a Relu activation function with an output size of 64, and the last one which is the output layer, uses a Softmax activation function to calculate the probability of each of the four classes. The algorithm hyperparameters are 10 epochs with batch size of 10 and Adam optimizer [38]. The DopplerNet algorithm was trained on dataset 1 yielding an accuracy higher than 90% as shown in Fig. 11 (b). When the trained algorithm is tested on dataset 2, its accuracy dropped to 50.25% as shown in Fig. 13 (a). This is the case for all previous works in which a ML algorithm was trained and tested on the same dataset that did not contain all possible mechanical control information, for example [37], [39]–[49]. But, if the classifier was trained on a dataset that covers *all* possible mechanical control information as shown in Fig. 1 (b), its accuracy would remain higher than 90% as shown in Fig. 13 (b), in this case the classifier was trained on dataset 1 and dataset 2 combined and tested on dataset 3.

For additional validation, a completely different dataset was generated using HFSS. The new dataset, dataset 4, contains random motions of the four drones at the following different rotors' speeds: 1000 RPM, 2000 RPM, 300 RPM, and 800 RPM. The trained MCML algorithm that covers all the mechanical control information of drones was applied to this new scenario, yielding an accuracy of at least 90%, as shown in Fig. 15. In the state-of-the-art literature, ML algorithms were trained on the hovering motion only of the drones, and few times they were trained on the hovering and pitching motions as reported in [37], [39]–[49].

A new scenario that contains random motions of the four drones was modeled in Ansys HFSS to create a dataset that contains range-Doppler images of the random motions for the four drones as shown in Fig. 16. The DopplerNet CNN classifier was trained on the hovering and pitching motions was trained solely on the hovering and pitching motions, following the approach employed

This article has been accepted for publication in IEEE Transactions on Aerospace and Electronic Systems. This is the author's version which has not been fully edited and content may change prior to final publication. Citation information: DOI 10.1109/TAES.2023.3272303

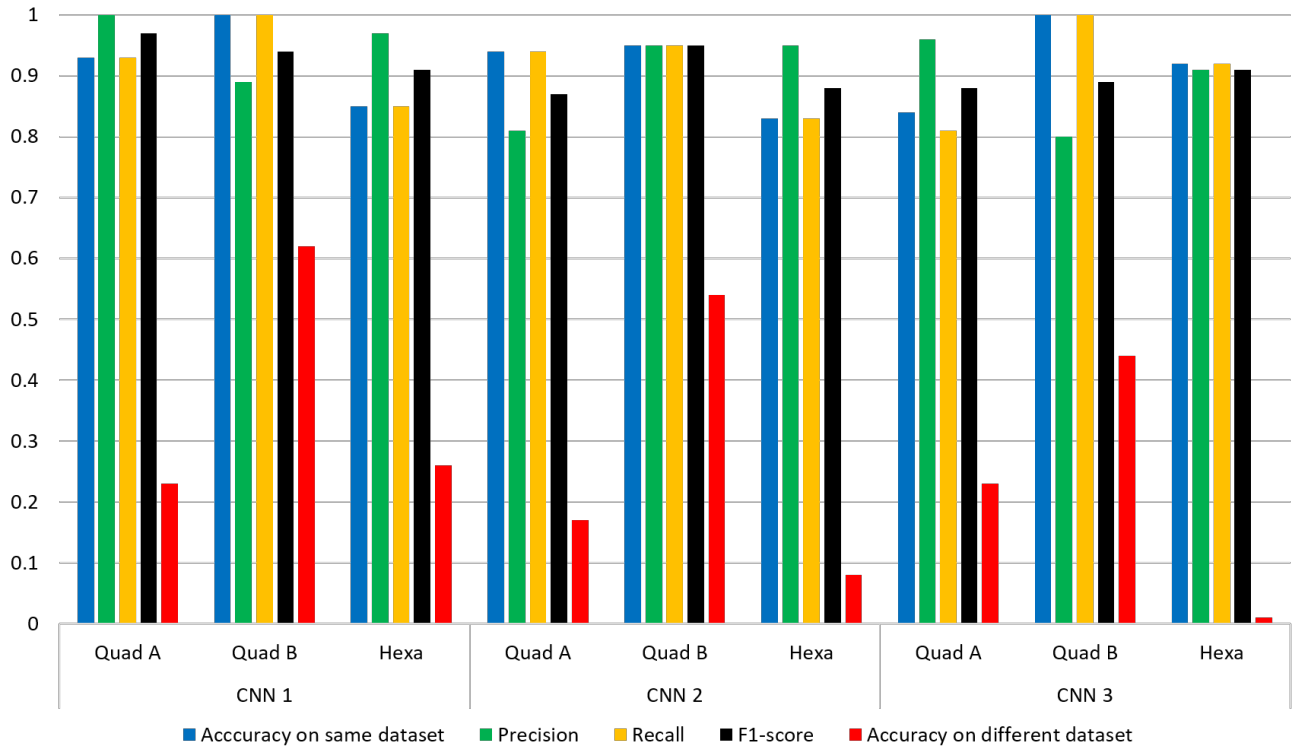

(a)

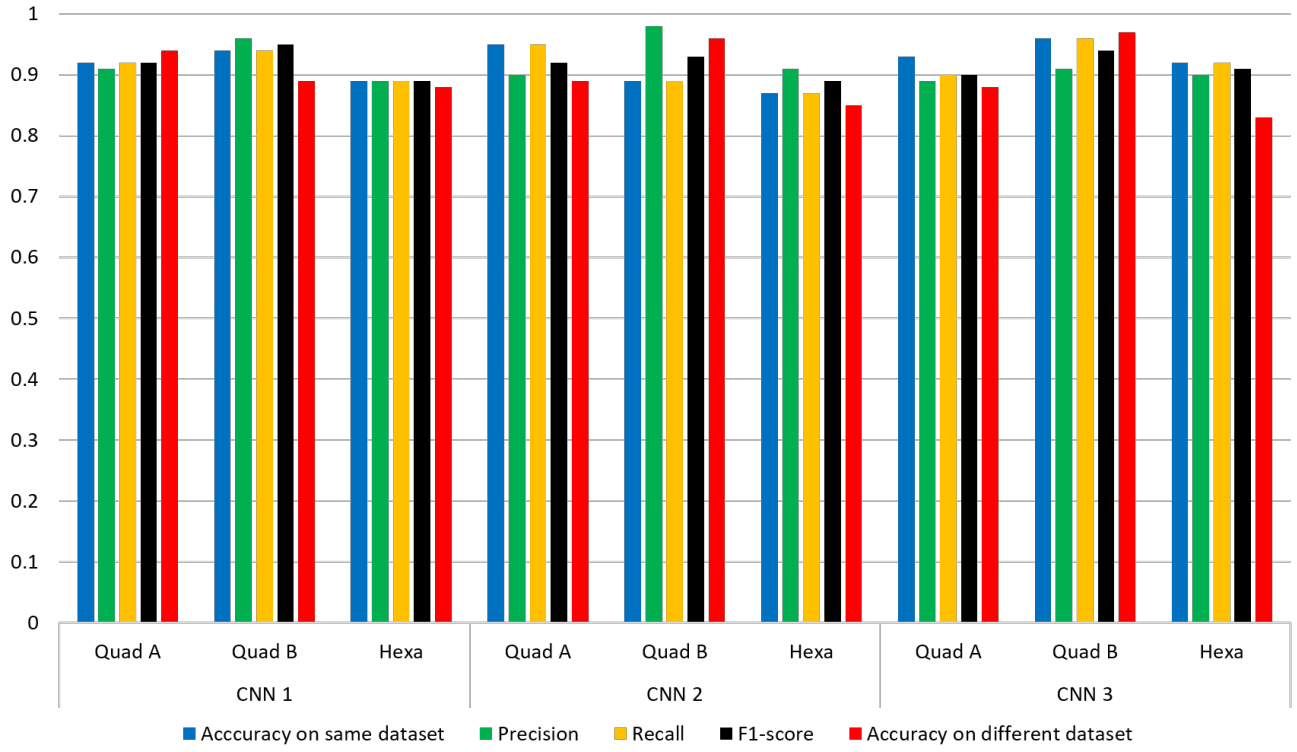

(b)

Fig. 14: Comparison of the classification reports for the three different CNN algorithms used in this work when (a) Not considering the mechanical control information of drones. (b) Considering the mechanical control information of drones.

in the current state-of-the-art literature [37], [39]–[49]. Then, the trained DopplerNet CNN classifier was applied to the generated dataset according to the scenario shown in Fig. 16, yielding an accuracy around 60%, as shown in Fig. 17 (a). Finally, the MCML algorithm, that consider *all* mechanical control information of drones, was applied

This article has been accepted for publication in IEEE Transactions on Aerospace and Electronic Systems. This is the author's version which has not been fully edited and content may change prior to final publication. Citation information: DOI 10.1109/TAES.2023.3272303

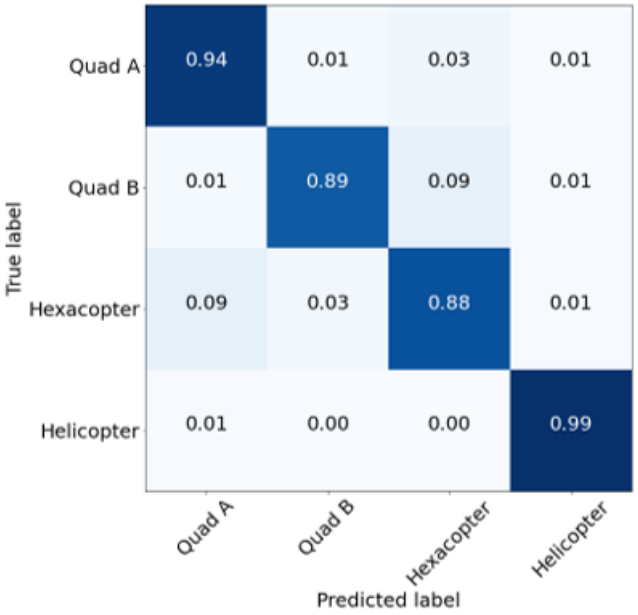

Fig. 15: A Confusion matrix for applying the proposed MCML algorithm to the new dataset.

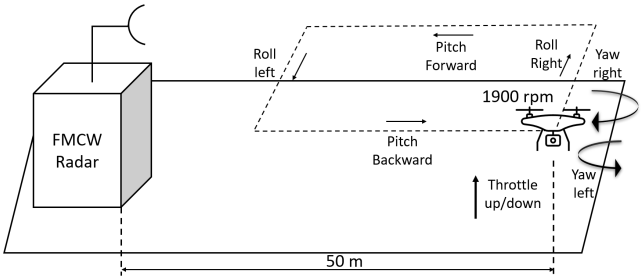

Fig. 16: HFSS simulation setup for all motions scenario.

to the same dataset giving an accuracy exceeding 97%, as shown in Fig. 17 (b).

The impact of the mechanical control information on the range-Doppler images of a real quadcopter was investigated using the AWR1443BOOST Texas Instruments (TI) radar [50]. The AWR1443BOOST TI radar, shown in Fig. 18 was used to generate range-Doppler images of throttling up and pitching forward motions for a DJI Phantom 3 standard quadcopter drone [51] as a proof of concept. The AWR1443BOOST TI radar operates at 76–81 GHz and possesses three transmitters and four receivers. Owing to the radar's internal Digital Signal Processing (DSP), received signals can be processed without the need for an external DSP system. To capture the Analog-to-Digital Converter (ADC) data and transmit it to a Personal Computer (PC), a DCA1000EVM board [52] was employed. The AWR1443BOOST radar configuration utilized for this investigation is presented in Table IV.

TABLE IV: The AWR1443BOOST TI Radar Configuration.

Quantity	Symbol	Value
Center Frequency	f_0	77 GHz
Bandwidth	BW	750 MHz
Range Resolution	ΔR	0.2 m
Velocity Resolution	ΔV	0.0694 m/s
Maximum Range	R_{max}	100 m

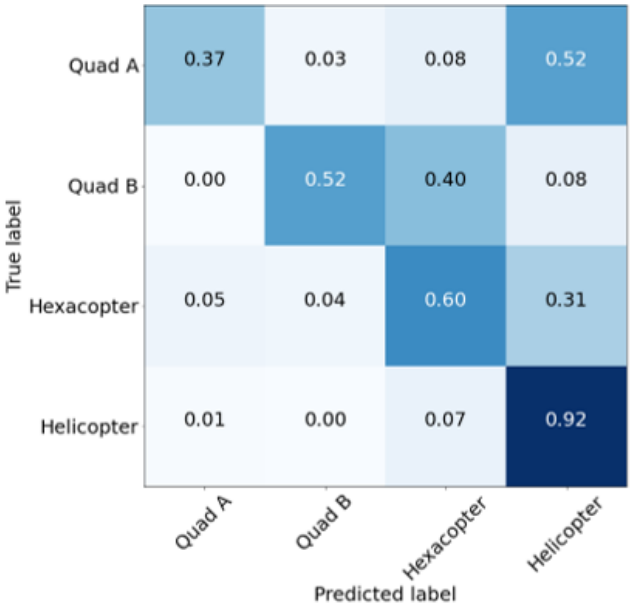

(a)

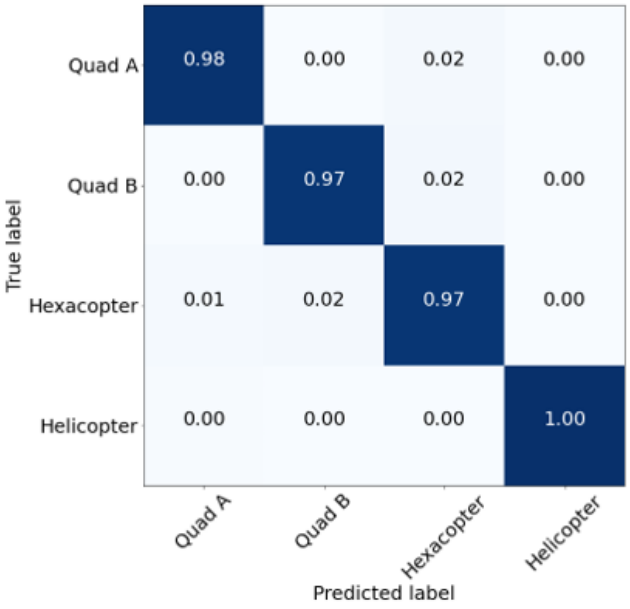

(b)

Fig. 17: A confusion matrix of applying the DopplerNet classifier on the full motions scenario according to (a) the state-of-the-art literature. (b) The proposed MCML method.

The DJI Phantom 3 standard drone was throttling up at a distance around 25 m in front of the AWR1443BOOST radar, as depicted in Fig. 19, then the DJI Phantom 3 standard drone started to pitch forward to the radar with a speed of 1.5 m/s. Fig. 20 (a) and Fig. 20 (b) show the range-Doppler images of the throttling up and pitching forward movements respectively. These images were obtained by applying a stationary clutter removal algorithm, followed by a FFT on the fast-time axis of the received signal to obtain the range information. A second FFT was then applied to the slow-time axis of the signal to extract the doppler velocity of the DJI Phantom 3 standard drone.

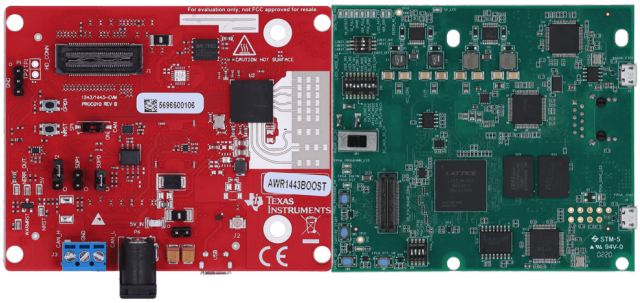

Fig. 18: The AWR1443BOOST TI radar (left in red) [50] and the DCA1000EVM board (right in green) [52].

Fig. 19: Measurements setup of the DJI Phantom 3 standard quadcopter.

The range-Doppler images depicted in Fig. 20, which are consistent with the range-Doppler images generated for the MD4-1000 quadcopter using Ansys HFSS as illustrated in Fig. 8 (a, c), highlight the strong dependence of range-Doppler images of drones on their mechanical control information.

V. CONCLUSION

The effect of the mechanical control information on the range-Doppler images for two quadcopters, a hexacopter, and a helicopter UAVs was introduced. A full-wave electromagnetic CAD tool is used to investigate these effects. The range-Doppler signatures are demonstrated to be highly dependent on mechanical control information for each drone. The mechanical control information for the four drones was employed using eight different classifiers to investigate their impact on classifying the four drones. The proposed MCML method overcomes the degraded classification accuracy in case the mechanical control information of UAVs was not taken into consideration. The MCML method provides classifier accuracy higher than 90%. High accuracy was also achieved when the trained MCML algorithm was applied to an unseen dataset containing random motions

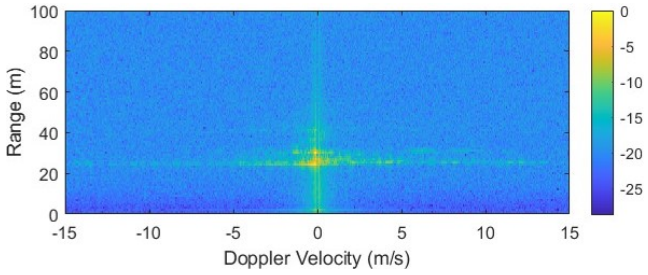

(a)

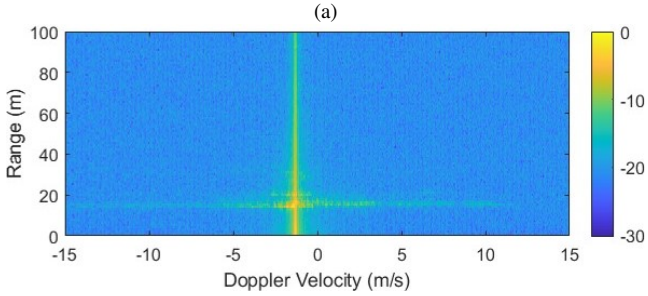

(b)

Fig. 20: (a) RD image of a throttling up DJI Phantom 3 standard. (b) RD image of a pitching forward DJI Phantom 3 standard.

of the four drones with different rotors' speeds. Overall, the proposed MCML method demonstrated superior accuracy when compared to state-of-the-art works employing radars for drone classification.

ACKNOWLEDGMENT

This work was supported in part by NSERC under Grant 55059. We would like to acknowledge CMC Microsystems and Ansys for providing the CAD tools licenses required for this work.

REFERENCES

[1] Heathrow airport: Drone sighting halts departures - bbc news. [Online]. Available: https://www.bbc.com/news/uk-46803713

[2] Drone sightings keep closing london's airports - bloomberg. [Online]. Available: https://www.bloomberg.com/news/articles/2019-01-09/drone-sightings-keep-closing-london-s-airports

[3] Iraq assassination attempt signals new era of non-state drone attacks - middle east eye. [Online]. Available: https://www.middleeasteye.net/opinion/iraq-assassination-new-era-drone-non-state-actors

[4] Turkey closes diyarbakir airport for month after drone attack 'by pkk' - world - the times. [Online]. Available: https://www.thetimes.co.uk/article/turkey-closes-diyarbakir-airport-for-month-after-drone-attack-by-pkk-gmcj8skfz

[5] Drone attack in abu dhabi kills 3 wounds 6 - cbc news. [Online]. Available: https://www.cbc.ca/news/world/abu-dhabi-drone-attack-1.6317555

[6] Shrapnel injures 12 at saudi abha airport as drone intercepted - reuters. [Online]. Available: https://www.reuters.com/world/middle-east/saudi-led-coalition-says-destroyed-drone-launched-towards-abha-airport-4-injured-2022-02-10/

[7] Flights diverted at east midlands airport after drone sightings - air transport - the guardian. [Online]. Available: https://www.theguardian.com/world/2022/jun/11/flights-diverted-at-east-midlands-airport-after-drone-sightings

[8] Rcmp charge two from b.c. after drone used to smuggle drugs into prison - ctv news. [Online]. Available: https:

//winnipeg.ctvnews.ca/drone-used-to-smuggle-drugs-into-manitoba-prison-rcmp-charge-two-men-from-b-c-1.5980061

[9] Small drones are giving ukraine an unprecedented edge - wired. [Online]. Available: https://www.wired.com/story/drones-russia-ukraine-war/

[10] Ukraine: How drones are changing the way of war - science - in-depth reporting on science and technology - dw. [Online]. Available: https://www.dw.com/en/ukraine-how-drones-are-changing-the-way-of-war/a-61681013

[11] G. Lykou, D. Moustakas, and D. Gritzalis
Defending airports from uas: A survey on cyber- attacks and counter-drone sensing technologies
Sensors, vol. 20, pp. 1–35, 6 2020.

[12] S. Park, H. T. Kim, S. Lee, H. Joo, and H. Kim
Survey on anti-drone systems: Components, designs, and challenges
IEEE Access, vol. 9, pp. 42 635–42 659, 2021.

[13] S. Samaras *et al.*
Deep learning on multi sensor data for counter uav applications—a systematic review
Sensors, vol. 19, 11 2019.

[14] J. Flórez, J. Ortega, A. Betancourt, A. García, M. Bedoya, and J. S. Botero
A review of algorithms, methods, and techniques for detecting uavs and uas using audio, radiofrequency, and video applications
TecnoLógicas, vol. 23, pp. 269–285, 5 2020.

[15] A. Sedunov, D. Haddad, H. Salloum, A. Sutin, N. Sedunov, and A. Yakubovskiy
Stevens drone detection acoustic system and experiments in acoustics uav tracking
2019 IEEE International Symposium on Technologies for Homeland Security, HST 2019, 11 2019.

[16] V. Balachandran and S. Sarath
A novel approach to detect unmanned aerial vehicle using pix2pix generative adversarial network
Proceedings of the 2nd International Conference on Artificial Intelligence and Smart Energy, ICAIS 2022, pp. 1368–1373, 2022.

[17] K. B. Kang, J. H. Choi, B. L. Cho, J. S. Lee, and K. T. Kim
Analysis of micro-doppler signatures of small uavs based on doppler spectrum
IEEE Transactions on Aerospace and Electronic Systems, vol. 57, pp. 3252–3267, 10 2021.

[18] H. Sun, B. S. Oh, X. Guo, and Z. Lin
Improving the doppler resolution of ground-based surveillance radar for drone detection
IEEE Transactions on Aerospace and Electronic Systems, vol. 55, pp. 3667–3673, 12 2019.

[19] B. S. Oh and Z. Lin
Extraction of global and local micro-doppler signature features from fmcw radar returns for uav detection
IEEE Transactions on Aerospace and Electronic Systems, vol. 57, pp. 1351–1360, 4 2021.

[20] A. N. Sayed, M. M. Y. R. Riad, O. M. Ramahi, and G. Shaker
A methodology for uav classification using machine learning and full-wave electromagnetic simulations
2022 International Telecommunications Conference (ITC-Egypt), pp. 1–2, 8 2022.

[21] Ansys hfss — 3d high frequency simulation software. [Online]. Available: https://www.ansys.com/products/electronics/ansys-hfss

[22] Z. Cendes
The development of hfss
2016 USNC-URSI Radio Science Meeting, 2016.

[23] Microdrones md4-1000 full specifications & reviews. [Online]. Available: https://productz.com/en/microdrones-md4-1000/p/y5RW

[24] Dji fpv - specs - dji. [Online]. Available: https://www.dji.com/ca/dji-fpv/specs

[25] Spreading wings s900 - dji. [Online]. Available: https://www.dji.com/ca/spreading-wings-s900

[26] Unmanned helicopter, small rotary, tactical uav, isr drones, ruav. [Online]. Available: https://www.unmannedsystemstechnology.com/company/steadicopter/

[27] S. W. Lee
Shooting and bouncing rays: Calculating the rcs of an arbitrarily shaped cavity
IEEE Transactions on Antennas and Propagation, vol. 37, pp. 194–205, 1989.

[28] S. K. Kim and D. M. Tilbury
Mathematical modeling and experimental identification of an unmanned helicopter robot with flybar dynamics
Journal of Robotic Systems, vol. 21, pp. 95–116, 3 2004.

[29] P. Wang, Z. Man, Z. Cao, J. Zheng, and Y. Zhao
Dynamics modelling and linear control of quadcopter
International Conference on Advanced Mechatronic Systems, ICAMechS, vol. 0, pp. 498–503, 7 2016.

[30] E. Bekir
Introduction to modern navigation systems. World scientific, 2007.

[31] K. Singh
Modelling and controls of a hexacopter
Master's thesis, Texas A&M University-Kingsville, 2018.

[32] A. Alaimo, V. Artale, C. Milazzo, A. Ricciardello, and L. Trefiletti
Mathematical modeling and control of a hexacopter
2013 International Conference on Unmanned Aircraft Systems, ICUAS 2013 - Conference Proceedings, 2013.

[33] K. S. Khuwaja, B. S. Chowdhry, K. F. Khuwaja, V. O. Mihalca, and R. C. Ţarcă
Virtual reality based visualization and training of a quadcopter by using rc remote control transmitter
IOP Conference Series: Materials Science and Engineering, vol. 444, p. 052008, 11 2018.

[34] I. Roldan *et al.*
Dopplernet: A convolutional neural network for recognising targets in real scenarios using a persistent range-doppler radar
IET Radar, Sonar and Navigation, vol. 14, pp. 593–600, 4 2020.

[35] S. Yoon *et al.*
Efficient protocol to use fmcw radar and cnn to distinguish micro-doppler signatures of multiple drones and birds
IEEE Access, vol. 10, pp. 26 033–26 044, 2022.

[36] K. Simonyan and A. Zisserman
Very deep convolutional networks for large-scale image recognition
3rd International Conference on Learning Representations, ICLR 2015 - Conference Track Proceedings, 9 2014.

[37] J. Park, J.-S. Park, and S.-O. Park
Small drone classification with light cnn and new micro-doppler signature extraction method based on a-spc technique
Arxiv, 9 2020.

[38] D. P. Kingma and J. Ba
Adam: A method for stochastic optimization
arxiv, 12 2014.

[39] B. K. Kim, H. S. Kang, and S. O. Park
Drone classification using convolutional neural networks with merged doppler images
IEEE Geoscience and Remote Sensing Letters, vol. 14, pp. 38–42, 1 2017.

[40] P. Zhang, L. Yang, G. Chen, and G. Li
Classification of drones based on micro-doppler signatures with dual-band radar sensors
Progress in Electromagnetics Research Symposium, vol. 2017-November, pp. 638–643, 11 2017.

[41] P. K. Rai *et al.*
Localization and activity classification of unmanned aerial vehicle using mmwave fmcw radars

IEEE Sensors Journal, vol. 21, pp. 16 043–16 053, 7 2021.

[42] P. Zhang, G. Li, C. Huo, and H. Yin
Exploitation of multipath micro-doppler signatures for drone classification
IET Radar, Sonar & Navigation, vol. 14, pp. 586–592, 4 2020.

[43] W. Zhang, G. Li, and C. Baker
Radar recognition of multiple micro-drones based on their micro-doppler signatures via dictionary learning
IET Radar, Sonar & Navigation, vol. 14, pp. 1310–1318, 9 2020.

[44] S. Rahman and D. Robertson
Time-frequency analysis of millimeter-wave radar micro-doppler data from small uavs
2017 Sensor Signal Processing for Defence Conference, SSPD 2017, vol. 2017-January, pp. 1–5, 12 2017.

[45] C. J. Li and H. Ling
An investigation on the radar signatures of small consumer drones
IEEE Antennas and Wireless Propagation Letters, vol. 16, pp. 649–652, 2017.

[46] H. C. Kumawat, M. Chakraborty, A. A. B. Raj, and S. V. Dhavale
Diat-μsat: Small aerial targets' micro-doppler signatures and their classification using cnn
IEEE Geoscience and Remote Sensing Letters, vol. 19, 2021.

[47] J. S. Patel, C. Al-Ameri, F. Fioranelli, and D. Anderson
Multi-time frequency analysis and classification of a micro-drone carrying payloads using multistatic radar
The Journal of Engineering, vol. 2019, pp. 7047–7051, 10 2019.

[48] M. Ritchie, F. Fioranelli, H. Borrion, and H. Griffiths
Multistatic micro-doppler radar feature extraction for classification of unloaded/loaded micro-drones
IET Radar, Sonar and Navigation, vol. 11, pp. 116–124, 2017.

[49] G. J. Mendis, T. Randeny, J. Wei, and A. Madanayake
Deep learning based doppler radar for micro uas detection and classification
Proceedings - IEEE Military Communications Conference MILCOM, pp. 924–929, 12 2016.

[50] Awr1443boost evaluation board. [Online]. Available: https://www.ti.com/tool/AWR1443BOOST

[51] Phantom 3 standard - dji. [Online]. Available: https://www.dji.com/ca/phantom-3-standard

[52] Dca1000evm evaluation board. [Online]. Available: https://www.ti.com/tool/DCA1000EVM

Ahmed N. Sayed (Graduate Student Member, IEEE) received the B.Sc. and M.Sc. degrees in electrical engineering in 2009 and 2015, respectively. He is currently pursuing the Ph.D. degree in electrical and computer engineering with the University of Waterloo, Waterloo, Ontario, Canada. Ahmed's research interests include radar detection, digital signal processing, radar signal processing, and machine learning.

Omar M. Ramahi (Fellow, IEEE) was born in Jerusalem, Palestine. He received the B.S. degrees (Highest Hons.) in mathematics and electrical and computer engineering from Oregon State University, Corvallis, Oregon, USA, in 1984, and the MS and Ph.D. degrees in electrical and computer engineering from the University of Illinois at Urbana–Champaign, Illinois, USA, in 1986 and 1990. He was with Digital Equipment Corporation (presently HP), MA, USA, where he was a member of the Alpha Server Product Development Group. In 2000, he joined the Faculty of the James Clark School of Engineering, the University of Maryland at College Park, MD, USA, as an Assistant Professor and later as a tenured Associate Professor, where he was also a Faculty Member of the CALCE Electronic Products and Systems Center. He is currently a Professor with the Department of Electrical and Computer Engineering, University of Waterloo, ON, Canada. He has authored and coauthored over 500 journal and conference technical articles on topics related to the electromagnetic phenomena and computational techniques. He has coauthored the book EMI/EMC Computational Modeling Handbook (first edition: Kluwer, 1998, Second Ed: Springer-Verlag, 2001. Japanese edition published in 2005). Prof. Ramahi received the 2004 University of Maryland Pi Tau Sigma Purple Cam Shaft Award. He received the Excellent Paper Award from the 2004 International Symposium on Electromagnetic Compatibility, Sendai, Japan, and the 2010 University of Waterloo Award for Excellence in Graduate Supervision. In 2012, he was a recipient of the IEEE EMC Society Technical Achievement Award. In 2022, Professor Ramahi was the winner of the 2022 University of Waterloo Engineering Research Excellence Award.

George Shaker (S IEEE 1997, SM IEEE 2015) is the lab director of the Wireless Sensors and Devices Laboratory at the University of Waterloo-Schlegel Research Institute for Aging. He is an (Adjunct + Research) professor with University of Waterloo at the Department of Electrical and Computer Engineering as well as the Department of Mechanical and Mechatronics Engineering. Previously, he was an NSERC scholar at Georgia Institute of Technology. Dr. Shaker also held multiple roles with RIM's (BlackBerry).

With close to twenty years of industrial experience in technology, and more than eight years as a faculty member leading project related to the application of wireless sensor systems for healthcare, automotives, and unmanned aerial vehicles, Prof. Shaker has many design contributions in commercial products available from startups and multinationals. A sample list includes Google, COM DEV, Honeywell, Blackberry, Konka, DBJ, Enice, Spark Tech Labs, China Mobile, TriL, Bionym, Lyngsoe Systems, ON Semiconductors, Ecobee, Medella Health, NERV Technologies, Novela, Thalmic Labs, North, General Dynamics Land Systems, General Motors, Toyota, Maple Lodge Farms, Rogers Communications, and Purolator.

Dr. Shaker has authored/coauthored 120+ publications and 35+ patents/patent applications. George has received multiple recognitions and awards, including the the IEEE AP-S Best Paper Award (the IEEE AP-S Honorable Mention Best Paper Award (4 times to-date), the IEEE Antennas and Propagation Graduate Research Award (the IEEE MTT-S Graduate Fellowship, the Electronic Components and Technology Best of Session paper award, and the IEEE Sensors most popular paper award. Two papers he co-authored in IEEE journals were among the top 25 downloaded papers on IEEEXplore for several consecutive months. He was the supervisor of the student team winning the third best design contest at IEEE AP-S 2016, co-author of the ACM MobileHCI 2017 best workshop paper award, and the 2018 Computer Vision Conference Imaging Best Paper Award. He co-received with his students several research recognitions including the NSERC Top Science Research Award 2019, IEEE APS HM paper award 2019, Biotec top demo award 2019, arXiv top downloaded paper (medical device category) 2019, Velocity fund 2020, NASA Tech Briefs HM Award (medical device category) 2020, UW Concept 2021, UK Dragons Canadian Competition 2021, CMC Nano 2021, COIL COLAB 2022, and Wiley Engineering Reports top downloaded paper for 2022.